Iranian Journal of Organic Chemistry Vol. 9, No. 2(2017) 2067-2077

DFT study of [^{18}F]flubatine

Mehdi Nabati[a,*], Maliheh-alsadat Kermanian[b], Ahmad Maghsoudloo-Mahalli[c] and Saman Sarshar[d]

[a]*Chemistry Department, Faculty of Science, Azarbaijan Shahid Madani University, Tabriz, Iran*
[b]*English language Department, Faculty of Foreign Languages, Pishva Branch, Islamic Azad University, Varamin, Iran*
[c]*Medical Radiation Department, Faculty of Nuclear Engineering, Central Tehran Branch, Islamic Azad University, Tehran, Iran*
[d]*Physics Department, Faculty of Science, Lorestan University, Khorramabad, Iran*

Received: February 2017; Revised: March 2017; Accepted: April 2017

Abstract: In the present article, the structural, electronic, reactivity and spectral properties of the nuclear medicine [^{18}F]flubatine have been studied using the density functional theory (DFT) technique. All computations were done by Gaussian 03 program using B3LYP computational method at 6-31+G(d,p) basis set. Firstly, the molecular structure was optimized at mentioned level of theory. In vibrational frequencies calculation, no imaginary frequency was shown. To study of the stability and reactivity of the molecule, the frontier molecular orbital theory was carried out. Our results for structural and electronic properties are compared with the experimental and other theoretical results wherever these are available.

Keywords: DFT study, [^{18}F]flubatine, Nuclear medicine, Radiopharmaceutical, Reactivity, Stability.

Introduction

Like all types of dementia, Alzheimer's is caused by brain cell death. It is a neurodegenerative disease, which means there is progressive brain cell death that happens over a course of time. The most common early symptom is difficulty in remembering recent events (short-term memory loss). As the disease advances, symptoms can include problems with language, disorientation (including easily getting lost), mood swings, loss of motivation, not managing self-care, and behavioral issues. As a person's condition declines, they often withdraw from family and society. Gradually, bodily functions are lost, ultimately leading to death. Although the speed of progression can vary, the average life expectancy following diagnosis is three to nine years.

*Corresponding author. Tel: +98 (413) 4327501, Fax: +98 (413) 4327501, E-mail: mnabati@ymail.com

The cause of Alzheimer's disease (AD) is poorly understood. About 70% of the risk is believed to be genetic with many genes usually involved. Other risk factors include a history of head injuries, depression, or hypertension. The disease process is associated with plaques and tangles in the brain. A probable diagnosis is based on the history of the illness and cognitive testing with medical imaging and blood tests to rule out other possible causes. Initial symptoms are often mistaken for normal ageing. Examination of brain tissue is needed for a definite diagnosis. Mental and physical exercise and avoiding obesity may decrease the risk of AD; however, evidence to support these recommendations is not strong [1-3].

The nicotinic α4β2 acetylcholine receptor is an important target for diagnostic neuroimaging and drug development because of its involvement in learning and memory processes, neuropsychiatric diseases such as alzheimer's disease (AD), parkinsons's disease (PD), Tourette's syndrome, epilepsy, autism, attention-deficit hyperactivity disorder, schizophrenia, and depression, as well as drug addiction and pain. In our group, highly

affine and selective α4β2nAChR targeting radiotracers have been developed which are related to the structure of the alkaloid epibatidine. The two radiolabeled enantiomers of norchloro-fluoro-homoepibatidine (NCFHEB), (+)-[^{18}F]flubatine and (-)-[^{18}F]flubatine, were investigated in piglets in dynamic positron emission tomography (PET) studies. (-)-[^{18}F]flubatine proofed to possess radiotracer properties superior to the clinically used 2-[^{18}F]F-A85380, and was already assessed in man to quantitatively image α4β2nAChR in the living brain. The other enantiomer (+)-[^{18}F]flubatine is currently also under investigation in patients with Alzheimer's disease [4-6].

Computational chemistry is a branch of chemistry that uses computer simulation to assist in solving chemical problems. It uses methods of theoretical chemistry, incorporated into efficient computer programs, to calculate the structures and properties of molecules and solids. Computational studies, used to find a starting point for a laboratory synthesis, or to assist in understanding experimental data, such as the position and source of spectroscopic peaks. Theoretical studies also used to predict the possibility of so far entirely unknown molecules or to explore reaction mechanisms not readily studied via experiments. Thus, computational chemistry can assist the experimental chemist or it can challenge the experimental chemist to find entirely new chemical objects [7-9]. Here, in the present study we investigate the structural properties, reactivity and spectra data analysis of the (1*R*,5*S*,6*S*)-6-(6-(fluoro-^{18}*F*)pyridin-3-yl)-8-azabicyclo[3.2.1]octane ([^{18}F]flubatine) by density functional theory (DFT) computational method.

Results and discussion

Structural properties of [^{18}F]flubatine:

[^{18}F]flubatine is a nuclear medicine which is used as a radiopharmaceutical for AD and PD diseases. Scheme **1** shows the molecular structure of this molecule with atomic numbering. The mentioned molecule was optimized by density functional theory (DFT) method at B3LYP functional with 6-31+G(d,p) level of theory. The optimized molecular structure of the compound is shown in Figure **1**. The bond lengths, bond angles and dihedral angles data of the molecule are listed in Table **1**. As can be seen from the data, the length of C-C bonds of the tricycle backbone is in 1.54-1.58 Å range. The C-C bonds length shows the order of C2-C3 > C3-C4 > C4-C6 > C1-C9 > C5-C9 > C1-C2 = C6-C5. The C-H bonds length in tricycle backbone is about 1.09 Å. Also, the length of the C-H, C-F, and C-C and C-N bonds in benzene ring of the structure is about 1.85, 1.35, 1.40 and 1.35 Å, respectively. In other hand, the bond angles data of the tricyclic segment of the structure indicates that all bond angles are lower than 120 degree. So, the bonds in this segment are under the angular pressure.

From the data of the Table **2**, the bond order (B.O.) of the C1-C9 and C5-C9 bonds is 1.011. Also, the B.O. of the C1-C2, C2-C3, C3-C4, C4-C6 and C6-C5 bonds is about 0.98-1.00. So, these bonds are weaker than the C1-C9 and C5-C9 bonds. In other hand, the C-H bonds order of the tricyclic backbone is about 0.9. It can be concluded from these bond orders that the C-H bonds of the tricyclic backbone of the structure have acidic property. Also, the N7-H8 bond of this backbone is more acidic than the C-H bonds, because of the of its bond order (about 0.8).

Table **3** indicates the natural bond orbitals (NBOs) population analysis data of the studied molecule. We can see the carbon atoms in the tricyclic backbone show more p and s orbitals for C-H and C-C bonds, respectively. This happens to reduce the angular pressure in the tricyclic backbone of the molecular structure. So, the more p orbital in carbon atoms of the C-H bonds causes the acidic property of these bonds.

Reactivity prediction of [^{18}F]flubatine:

In this section of research work, the molecular orbital (MO) theory of the studied molecule is explored. In chemistry, frontier molecular orbital (FMO) theory is an application of MO theory describing HOMO/LUMO interactions [10]. The images of the frontier molecular orbitals of this compound are shown in Figure **2**. It can be seen from the HOMO/LUMO graphs, the lowest unoccupied molecular orbitals are on the benzene ring of the molecule. So, this segment of the compound is more reactive than another segment (tricyclic backbone). From the DFT computations, the energies of the HOMO and LUMO orbitals are -6.48 and -1.35 eV, respectively. The energies gap of the HOMO/LUMO orbitals is 5.13 eV. This energies gap proves that the molecule is a stable compound. The graph of the density of states (DOS) of the molecule shows us that the unoccupied orbitals have more states than the occupied molecules, but they have more energy. So, this molecule is a stable compound and it can't react with electrophiles. In other hand, the DOS of the occupied molecular orbitals shows that this compound can react with nucleophiles.

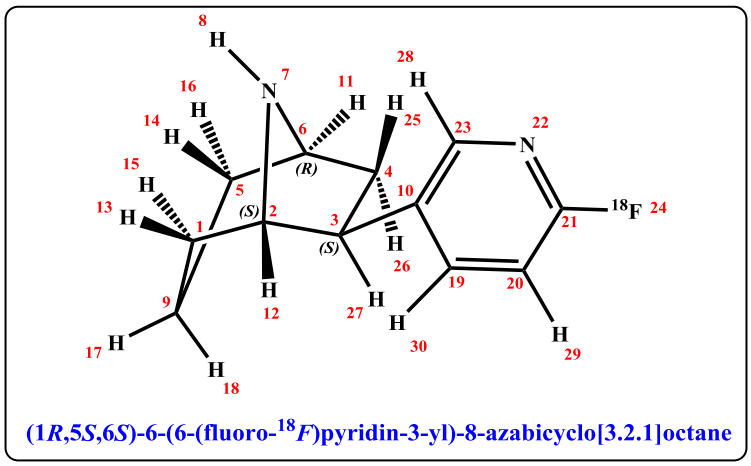

Scheme 1. The molecular structure of [^{18}F]flubatine.

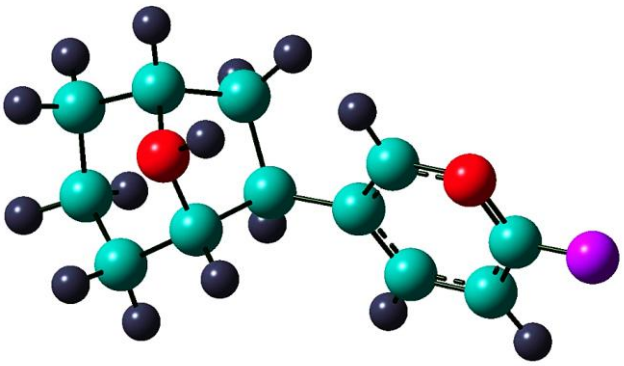

Figure 1. The optimized structure of [^{18}F]flubatine.

Table 1. Bond lengths, bond angles and dihedral angles data of the studied molecule.

Bonds	Bond length (Angstrom)	Bond angle	Angle (degree)
C1-C2	1.540	C1-C2-C3	111.428
C2-C3	1.581	C2-C3-C4	102.509
C3-C4	1.562	C3-C4-C6	104.654
C4-C6	1.559	C4-C6-C5	112.642
C6-C5	1.540	C6-C5-C9	111.167
C5-C9	1.542	C5-C9-C1	111.897
C1-C9	1.543	C9-C1-C2	111.339
C6-N7	1.479	C1-C2-N7	107.137
C2-N7	1.473	C3-C2-N7	105.654
C1-H13	1.097	C4-C6-N7	104.785
C1-H15	1.096	C5-C6-N7	107.050
C2-H12	1.094	C2-N7-C6	102.334
C3-H27	1.096	C3-C10-C23	123.338
C4-H25	1.094	C3-C10-C19	120.606
C4-H26	1.095	C10-C23-N22	124.375
C6-H11	1.095	C23-N22-C21	116.961
N7-H8	1.018	N22-C21-C20	125.510
C5-H14	1.096	C21-C20-C19	116.465

C5-H16	1.097	C20-C19-C10	120.684
C9-H17	1.096	C19-C10-C23	116.003
C9-H18	1.098	N22-C21-F24	116.212
C3-C10	1.516	C20-C21-F24	118.277
C10-C19	1.406	H25-C4-C3-C10	5.640
C19-C20	1.391	H26-C4-C3-C10	113.350
C20-C21	1.394	H25-C4-C3-H27	126.634
C21-N22	1.311	H26-C4-C3-H27	7.644
N22-C23	1.344	C3-C10-C23-H28	3.703
C10-C23	1.401	C3-C10-C19-H30	2.983
C19-H30	1.087	H11-C6-N7-H8	47.190
C20-H29	1.084	H12-C2-N7-H8	46.766
C21-F24	1.354	N7-C2-C3-C10	99.909
C23-H28	1.087	H12-C2-C3-C10	20.141

Table 2. Bond orders (B.O.) data of the studied molecule.

Bonds	Bond order (B.O.)	Bonds	Bond order (B.O.)
C1-C2	0.997	N7-H8	0.815
C2-C3	0.944	C5-H14	0.906
C3-C4	0.988	C5-H16	0.914
C4-C6	0.983	C9-H17	0.910
C6-C5	0.998	C9-H18	0.916
C5-C9	1.011	C3-C10	1.015
C1-C9	1.011	C10-C19	1.382
C6-N7	0.980	C19-C20	1.463
C2-N7	0.990	C20-C21	1.359
C1-H13	0.914	C21-N22	1.451
C1-H15	0.904	N22-C23	1.389
C2-H12	0.900	C10-C23	1.413
C3-H27	0.899	C19-H30	0.907
C4-H25	0.915	C20-H29	0.899
C4-H26	0.913	C21-F24	0.877
C6-H11	0.902	C23-H28	0.908

Figure **4** shows the molecular electrostatic potential (MEP) graph of the molecule. In this molecule, the colors have been chosen such that regions of attractive potential appear in red and those of repulsive potential appear in green. The Figure shows that the nitrogen and fluorine atoms are more reactive sites of this molecule.

CD, UV-Vis, IR and NMR spectra prediction of [^{18}F]flubatine:

There are several spectroscopic techniques which can be used to identify organic molecules: infrared (IR), mass spectroscopy (MS) UV-Visible spectroscopy (UV-Vis) and nuclear magnetic resonance (NMR). IR, NMR and UV-Vis spectroscopy are based on observing the frequencies of electromagnetic radiation absorbed and emitted by molecules [11-14].

Circular dichroism (CD) is dichroism involving circularly polarized light, i.e., the differential absorption of left- and right-handed light. Left-hand circular (LHC) and right-hand circular (RHC) polarized light represent two possible spin angular momentum states for a photon, and so circular dichroism is also referred to as dichroism for spin angular momentum. This phenomenon was discovered by Jean-Baptiste Biot, Augustin Fresnel, and Aimé Cotton in the first half of the 19th century. It is exhibited in the absorption bands of optically active chiral molecules. Measurements carried out in the visible and ultra-violet region of the electro-magnetic spectrum monitor electronic transitions, and, if the molecule under study contains chiral chromophores

then one circularly polarized light (CPL) state will be absorbed to a greater extent than the other and the CD signal over the corresponding wavelengths will be non-zero. A circular dichroism signal can be positive or negative, depending on whether left-handed circularly polarized light (L-CPL) is absorbed to a greater extent than right-handed circularly polarized light (R-CPL) (CD signal positive) or to a lesser extent (CD signal negative) [15]. It can be seen from the Figure **5**, [^{18}F]flubatine is a right-handed molecule. The UV-Vis spectrum of the studied compound is indicated in Figure **6**. In the UV-Vis spectrum, the peak at wavelength 275.948 nm with energy 36238.741 cm^{-1} is related to the HOMO to LUMO transition. The other transitions (HOMO to LUMO+1 (89%), HOMO-1 to LUMO (5%) and HOMO-1 to LUMO+1 (2%)) take place at wavelength 240.599 nm with energy 41562.843 cm^{-1}. Also, the HOMO-2 to LUMO transition is shown at wavelength 239.290 nm with energy 41790.293 cm^{-1}. Figure **7** indicates the IR spectrum of the studied molecule. IR [Harmonic frequencies (cm^{-1}), intensities (KM/Mole)]: 39.7150 (0.6019), 62.7313 (1.2204), 68.6222 (1.0299), 188.5924 (0.1663), 195.9007 (0.2693), 244.2866 (0.2108), 275.1305 (0.0832), 318.6722 (0.5665), 361.6087 (1.7348), 413.3038 (2.3839), 443.9687 (1.4445), 454.0157 (5.5457), 460.2061 (2.4925), 489.9394 (2.1730), 543.3140 (7.9684), 558.3616 (5.5750), 605.3335 (13.9940), 650.0902 (2.6077), 718.6430 (7.7336), 733.7757 (0.5209), 759.0369 (4.2574), 785.7326 (4.4531), 801.5511 (24.9203), 828.0829 (62.5263), 837.3687 (63.5228), 860.1795 (7.2255), 865.1391 (30.5170), 874.3292 (1.9523), 894.9098 (5.6289), 908.2242 (0.7857), 938.1893 (2.2158), 953.2852 (4.3906), 964.3124 (5.7624), 970.0223 (13.8821), 985.8205 (0.6025), 1041.0445 (9.9388), 1051.8493 (9.4968), 1061.33567 (0.6147), 1070.1151 (10.8951), 1099.4016 (17.3246), 1102.9475(12.7626), 1148.4516 (10.2640), 1161.5925 (0.1885), 1165.7891 (6.7403), 1201.7309 (7.4931), 1231.3796 (1.9271), 1249.7660 (3.0535), 1270.2592 (15.1612), 1274.1468 (43.5374), 1281.0179 (112.1375), 1292.0021 (4.0465), 1308.6999 (3.1785), 1316.4043 (0.5953), 1331.4784 (8.3160), 1338.8039 (3.8785 (3.8785), 1356.1201 (0.8196), 1367.1933 (15.3684), 1377.3442 (0.8912), 1384.6695 (1.9932), 1399.6766 (7.8850), 1438.0995 (31.0864), 1443.7755 (3.7496), 1482.2870 (2.3863), 1488.5641 (3.2220), 1500.7766 (7.3961), 1513.6376 (52.8080), 1521.8745 (151.3605), 1629.9660 (35.4934), 1640.4891 (45.1101), 3030.0265 (16.2994), 3037.1186 (47.1761), 3039.2571 (22.7924), 3055.4791 (22.2927), 3061.7554 (22.3312), 3068.7630 (44.4804), 3079.7324 (67.4186), 3082.9760 (1.6788), 3089.3178 (31.3048), 3090.6648 (65.9932), 3103.6641 (32.1452), 3180.4091 (23.5203), 3184.6647 (8.1771), 3226.6492 (2.6341), 3501.8174 (1.4812).

Table 2. Bond orders (B.O.) data of the studied molecule.

Bonds	Bond order (B.O.)	Bonds	Bond order (B.O.)
C1-C2	0.997	N7-H8	0.815
C2-C3	0.944	C5-H14	0.906
C3-C4	0.988	C5-H16	0.914
C4-C6	0.983	C9-H17	0.910
C6-C5	0.998	C9-H18	0.916
C5-C9	1.011	C3-C10	1.015
C1-C9	1.011	C10-C19	1.382
C6-N7	0.980	C19-C20	1.463
C2-N7	0.990	C20-C21	1.359
C1-H13	0.914	C21-N22	1.451
C1-H15	0.904	N22-C23	1.389
C2-H12	0.900	C10-C23	1.413
C3-H27	0.899	C19-H30	0.907
C4-H25	0.915	C20-H29	0.899
C4-H26	0.913	C21-F24	0.877
C6-H11	0.902	C23-H28	0.908

Table 3. Natural bond orbitals (NBOs) analysis data of the studied molecule.

Bonds	Occupancy	Population/Bond orbital/Hybrids
σ(C1-C2)	1.97847	49.11% C1 ($sp^{2.82}$), 50.89% C2 ($sp^{2.67}$)
σ(C1-H13)	1.98123	62.12% C1 ($sp^{3.22}$), 37.88% H13 (s)
σ(C1-H15)	1.97956	62.88% C1 ($sp^{3.24}$), 37.12% H15 (s)
σ(C1-C9)	1.98560	49.98% C1 ($sp^{2.78}$), 50.02% C9 ($sp^{2.77}$)
σ(C2-C3)	1.96393	48.47% C2 ($sp^{3.00}$), 51.53% C3 ($sp^{3.18}$)
σ(C2-H12)	1.98086	63.02% C2 ($sp^{2.88}$), 36.98% H12 (s)
σ(C2-N7)	1.98355	40.43% C2 ($sp^{3.57}$), 59.57% N7 ($sp^{2.53}$)
σ(C6-C5)	1.98079	50.81% C6 ($sp^{2.69}$), 49.19% C5 ($sp^{2.82}$)
σ(C6-C4)	1.98079	49.74% C6 ($sp^{2.85}$), 50.26% C4 ($sp^{2.91}$)
σ(C6-H11)	1.98044	62.85% C6 ($sp^{2.95}$), 37.15% H11 (s)
σ(C6-N7)	1.98337	40.32% C6 ($sp^{3.66}$), 59.68% N7 ($sp^{2.55}$)
σ(C5-H16)	1.98126	62.19% C5 ($sp^{3.21}$), 37.81% H16 (s)
σ(C5-H14)	1.98069	62.77% C5 ($sp^{3.23}$), 37.23% H14 (s)
σ(C5-C9)	1.98572	49.85% C5 ($sp^{2.78}$), 50.15% C9 ($sp^{2.76}$)
σ(C3-H27)	1.97680	62.78% C3 ($sp^{3.24}$), 37.22% H27 (s)
σ(C3-C4)	1.97272	51.30% C3 ($sp^{2.96}$), 48.70% C4 ($sp^{2.97}$)
σ(C3-C10)	1.97596	49.24% C3 ($sp^{2.66}$), 50.76% C10 ($sp^{1.99}$)
σ(C4-H25)	1.98434	62.45% C4 ($sp^{3.10}$), 37.55% H25 (s)
σ(C4-H26)	1.98487	62.63% C4 ($sp^{3.03}$), 37.37% H26 (s)
σ(C9-H18)	1.98187	61.71% C9 ($sp^{3.39}$), 38.29% H18 (s)
σ(C9-H17)	1.98297	62.72% C9 ($sp^{3.16}$), 37.28% H17 (s)
σ(N7-H8)	1.98178	70.13% N7 ($sp^{3.30}$), 29.87% H8 (s)
σ(C10-C19)	1.97535	50.63% C10 ($sp^{1.99}$), 49.37% C19 ($sp^{1.85}$)
σ(C10-C23)	1.97951	51.34% C10 ($sp^{2.03}$), 48.66% C23 ($sp^{1.61}$)
π(C10-C23)	1.63988	52.13% C10 ($sp^{99.99}d^{3.08}$), 47.87% C23 (p)
σ(C19-C20)	1.97457	49.89% C19 ($sp^{1.86}$), 50.11% C20 ($sp^{1.81}$)
π(C19-C20)	1.68593	46.95% C19 (p), 53.05% C20 (p)
σ(C19-H30)	1.98157	62.60% C19 ($sp^{2.34}$), 37.40% H30 (s)
σ(C23-H28)	1.98128	61.77% C23 ($sp^{2.26}$), 38.23% H28 (s)
σ(C23-N22)	1.97698	40.48% C23 ($sp^{2.22}$), 59.52% N22 ($sp^{1.78}d^{0.01}$)
σ(C20-C21)	1.98399	50.62% C20 ($sp^{2.11}$), 49.38% C21 ($sp^{1.38}$)
σ(C20-H29)	1.97954	63.32% C20 ($sp^{2.10}$), 36.68% H29 (s)
σ(C21-N22)	1.98662	40.75% C21 ($sp^{1.86}$), 59.25% N22 ($sp^{1.86}d^{0.01}$)
π(C21-N22)	1.73422	40.49% C21 (p), 59.51% N22 (p)
σ(C21-F24)	1.99506	27.46% C21 ($sp^{3.36}d^{0.01}$), 72.54% F24 ($sp^{2.41}$)
Lp (N7)	1.92015	N7 ($sp^{3.94}$)

Table 4. The ^{1}H and ^{13}C chemical shifts of the studied molecule.

Nucleus	Chemical Shift (ppm)	
	Theoretical chemical shifts ($\delta = \delta_{TMS} - \delta'$)	**δ (Chemical shifts from ChemBioDraw Ultra 13.0)**
H-8	2.179	2.000
H-11	3.524	2.650
H-12	2.854	3.030
H-13	1.459	1.440
H-14	1.956	1.440
H-15	1.876	1.440
H-16	1.389	1.440
H-17	1.531	1.500
H-18	1.639	1.500
H-25	1.867	1.950
H-26	2.371	1.700
H-27	3.104	2.770
H-28	8.142	8.200
H-29	6.841	7.190
H-30	7.555	7.970
C-1	35.640	31.300
C-2	71.168	82.200
C-3	52.841	38.400
C-4	44.242	34.400
C-5	35.362	32.900
C-6	62.294	59.100
C-9	22.673	20.800
C-10	139.550	136.600
C-19	137.257	142.200
C-20	105.400	109.400
C-21	161.939	163.100
C-23	142.267	147.000

The NMR technique is a good method for identification of the structure of the organic compounds [16, 17]. The ^{1}H and ^{13}C chemical shifts of the studied molecule are listed in Table **4**. The theoretical chemical shifts data is compared to the experimental values. The Figures **8** and **9** indicate the comparison between the theoretical and experimental ^{1}H and ^{13}C chemical shifts of the molecular structure at studied computational method. The large correlation coefficients (0.98 and 0.99 for hydrogen and carbon nucleus, respectively) show the accuracy of our computations. The data of the Table **4** indicates that the H12 and H11 nucleus are more de-shielded than the other hydrogen nucleus. Another de-shielded nucleus is C21 atom, because it connects to two electronegative atoms (nitrogen and fluorine atoms).

Computational method:

In present research work, all computations were performed by Gaussian 03 package [18] using density functional theory (DFT) computational method by B3LYP functional with 6-31+G(d,p) basis set. The computations were done in the gas phase at room temperature.

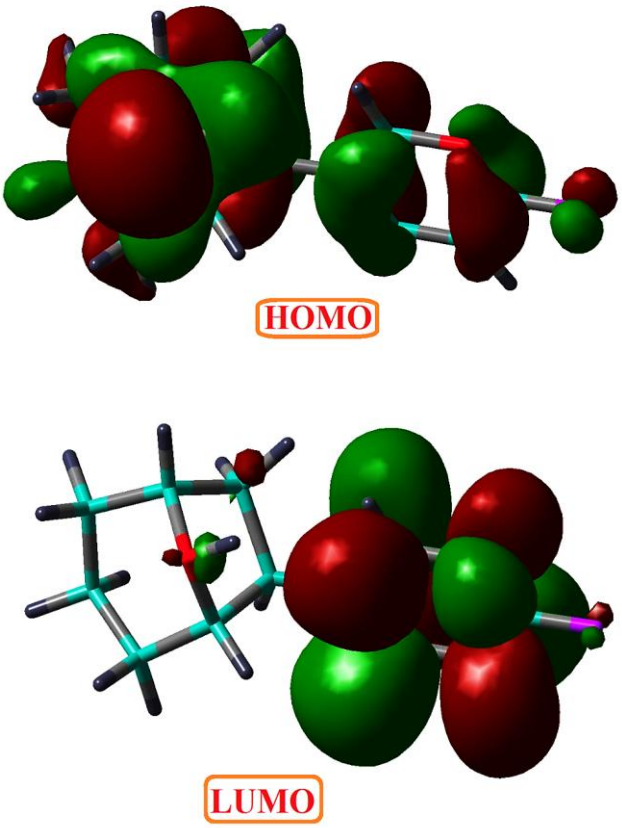

Figure 2. The frontier molecular orbitals of [^{18}F]flubatine.

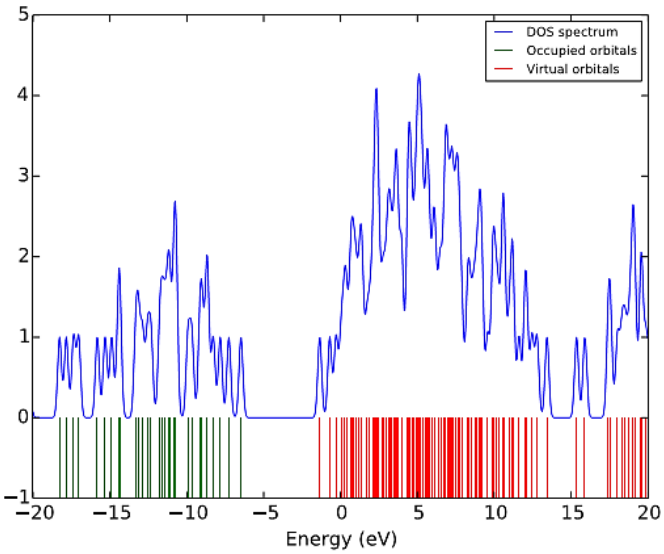

Figure 3. The density of states (DOS) graph of [^{18}F]flubatine.

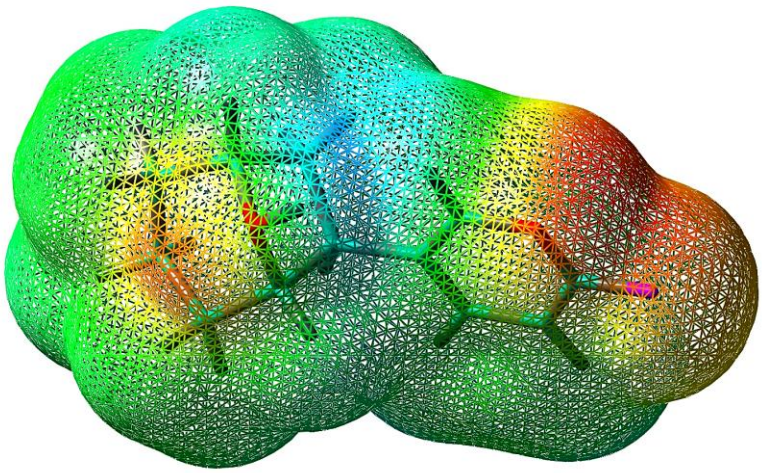

Figure 4. The molecular electrostatic potential (MEP) graph of [^{18}F]flubatine.

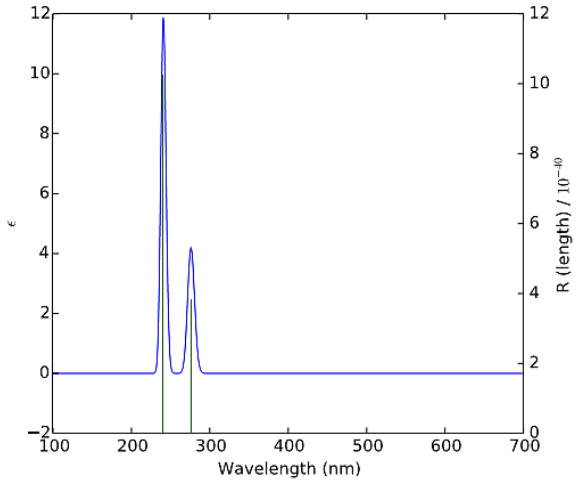

Figure 5. The CD spectrum of the studied molecule.

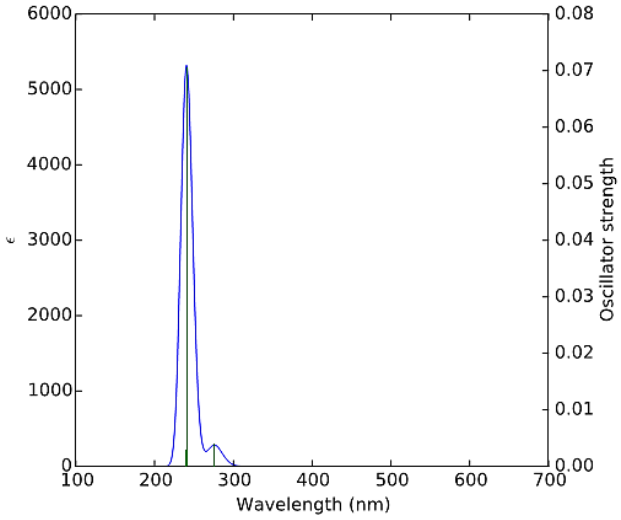

Figure 6. The UV-Vis spectrum of the studied molecule.

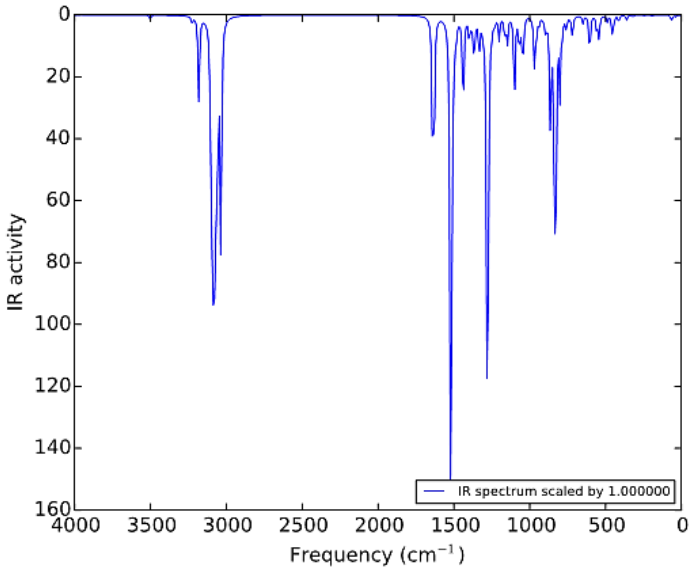

Figure 7. The IR spectrum of the studied molecule.

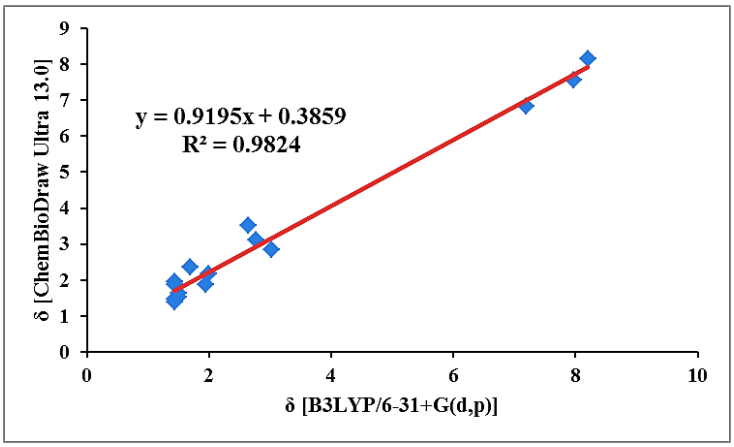

Figure 8. The relationship between theoretical and experimental ^{1}H chemical shifts of the studied structure.

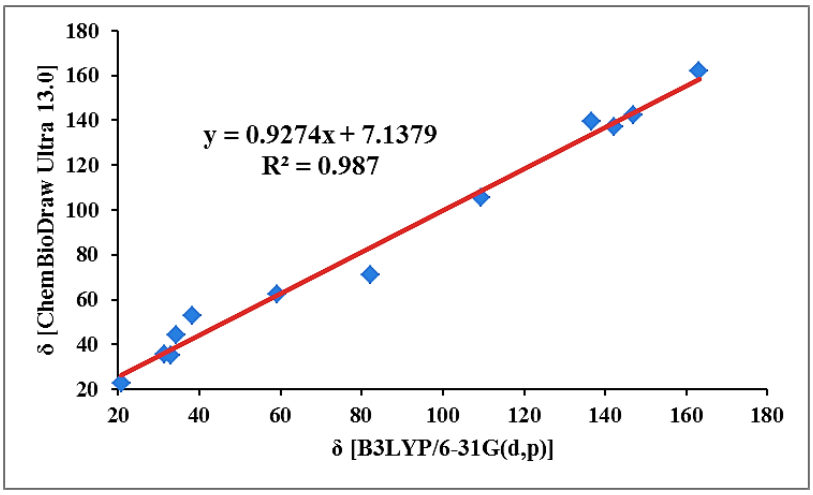

Figure 9. The relationship between theoretical and experimental ^{13}C chemical shifts of the studied structure.

Conclusions

In summary, in this present research work we have investigated the structural, electronic and spectral properties of [^{18}F]flubatine using B3LYP/6-31+G(d,p) level of theory. The main of this work was to study the structural properties (bond lengths, bond angles, dihedral angles and bond orders), natural bond orbitals (NBOs) population analysis, reactivity (frontier molecular orbitals analysis) and spectral analysis (CD, UV-Vis, IR and NMR spectroscopy techniques) of the studied molecular structure. In first step, the molecule was optimized at mentioned level of theory. Then, the other computations were done on the structure. The structural and spectral analysis data shows our computational method has a good accuracy to the experimental data. Also, the frontier molecular orbitals (FMOs) investigation indicates the molecule is stable and the benzene ring of the molecule is more reactive than another segment of the molecule. The MEP graph shows that the nitrogen and fluorine atoms of the compound are the more reactive sites of the structure.

Acknowledgments

The corresponding author is grateful to Doctor Hojjatollah Salehi and Mr. Hossein Abbasi for providing valuable suggestions.

References

[1] Fallahi, B.; Esmaeili, A.; Beiki, D.; Oveisgharan, S.; Noorollahi-Moghaddam, H.; Erfani, M.; Tafakhori, A.; Rohani, M.; Fard-Esfahani, A.; Emami-Ardekani, A.; Geramifar, P.; Eftekhari, M. *Ann. Nucl. Med.*, **2016**, *30*, 153-162.

[2] Erfani, M.; TShafiei, M. *Nucl. Med. Biol.*, **2014**, *30*, 317-321.

[3] Erfani, M.; TShafiei, M.; Charkhlooie, G.; Goudarzi, M. *Iran J. Nucl. Med.*, **2015**, *23*, 15-20.

[4] Fischer, S.; Hiller, A.; Smits, R.; Hoepping, A.; Funke, U.; Wenzel, B.; Cumming, P.; Sabri, O.; Steinbach, J.; Brust, P. *Appl. Radiat. Isot.*, **2013**, *74*, 128-136.

[5] Sabri, O.; Becker, G.; Meyer, P. M.; Hesse, S.; Wilke, S.; Graef, S.; Patt, M.; Luthardt, J.; Wagenknecht, G.; Hoepping, A. *J. Neurolmage*, **2015**, *118*, 199-208.

[6] Smits, R.; Fischer, S.; Hiller, A.; Deuther-Conrad, W.; Wenzel, B.; Patt, M.; Cumming, P.; Steinbach, J.; Sabri, O.; Brust, P.; Hoepping, A. *Bioorg. Med. Chem.*, **2014**, *22*, 804-812.

[7] Nabati, M. *J. Phys. Theor. Chem. IAU Iran*, **2015**, *12*, 325-338.

[8] Nabati, M.; Mahkam, M.; Atani, Y. G. *J. Phys. Theor. Chem. IAU Iran*, **2016**, *13*, 35-59.

[9] Nabati, M.; Mahkam, M. *Org. Chem. Res.*, **2016**, *2*, 70-80.

[10] Nabati, M. *Iran. J. Org. Chem.*, **2016**, *8*, 1703-1716.

[11] Nabati, M. *J. Phys. Theor. Chem. IAU Iran*, **2016**, *13*, 133-146.

[12] Nabati, M.; Mahkam, M. *J. Phys. Theor. Chem. IAU Iran*, **2015**, *12*, 33-43.

[13] Nabati, M.; Mahkam, M. *Silicon*, **2016**, *8*, 461-465.

[14] Nabati, M.; Mahkam, M. *J. Phys. Theor. Chem. IAU Iran*, **2015**, *12*, 121-136.

[15] Nabati, M.; Mahkam, M. *Iran. J. Org. Chem.*, **2015**, *7*, 1463-1472.

[16] Nabati, M.; Mofrad, M. H.; Kermanian, M.; Sarshar, S. *Iran. J. Org. Chem.*, **2017**, *9*, 1981-1993.

[17] Nabati, M.; Salehi, H. *Iran. J. Org. Chem.*, **2017**, *9*, 2013-2023.

[18] Frisch, M. J.; Trucks, G. W.; Schlegel, H. B.; Scuseria, G. E.; Robb, M. A.; Cheeseman, J. R.; Montgomery Jr., J. A.; Vreven, T.; Kudin, K. N.; Burant, J. C.; Millam, J. M.; Iyengar, S. S.; Tomasi, J.; Barone, V.; Mennucci, B.; Cossi, M.; Scalmani, G.; Rega, N.; Petersson, G. A.; Nakatsuji, H.; Hada, M.; Ehara, M.; Toyota, K.; Fukuda, R.; Hasegawa, J.; Ishida, M.; Nakajima, T.; Honda, Y.; Kitao, O.; Nakai, H.; Klene, M.; Li, X.; Knox, J. E.; Hratchian, H. P.; Cross, J. B.; Adamo, C.; Jaramillo, J.; Gomperts, R.; Stratmann, R. E.; Yazyev, O.; Austin, A. J.; Cammi, R.; Pomelli, C.; Ochterski, J. W.; Ayala, P. Y.; Morokuma, K.; Voth, G. A.; Salvador, P.; Dannenberg, J. J.; Zakrzewski, V. G.; Dapprich, S.; Daniels, A. D.; Strain, M. C.; Farkas, O.; Malick, D. K.; Rabuck, A. D.; Raghavachari, K.; Foresman, J. B.; Ortiz, J. V.; Cui, Q.; Baboul, A. G.; Clifford, S.; Cioslowski, J.; Stefanov, B. B.; Liu, G.; Liashenko, A; Piskorz, P.; Komaromi, I.; Martin, R. L.; Fox, D. J.; Keith, T.; Al-Laham, M. A.; Peng, C. Y.; Nanayakkara, A.; Challacombe, M.; Gill, P. M. W.; Johnson, B.; Chen, W.; Wong, M. W.; Gonzalez, C.; Pople, J. A. *Gaussian 03. Revision B.01*. Gaussian Inc. Wallingford. CT. **2004.**